Measurement of the Excitation Spectrum of a Dipolar Gas in the Macrodroplet Regime

J. J. A. Houwman,[1] D. Baillie,[2] P. B. Blakie,[2] G. Natale,[1,3] F. Ferlaino,[1,3] and M. J. Mark[1,3]
[1]Universität Innsbruck, Institut für Experimentalphysik, 6020 Innsbruck, Austria
[2]Department of Physics, Centre for Quantum Science, and The Dodd-Walls Centre for Photonic and Quantum Technologies, University of Otago, Dunedin 9016, New Zealand
[3]Institut für Quantenoptik und Quanteninformation, Österreichische Akademie der Wissenschaften, 6020 Innsbruck, Austria

(Received 28 July 2023; revised 27 November 2023; accepted 8 January 2024; published 7 March 2024)

The excitation spectrum of a cigar-shaped strongly dipolar quantum gas at the crossover from a Bose-Einstein condensate to a trapped macrodroplet is predicted to exhibit peculiar features—a strong upward shift of low momentum excitation energies together with a strong multiband response for high momenta. By performing Bragg spectroscopy over a wide range of momenta, we observe both key elements and also confirm the predicted stiffening of excitation modes when approaching the macrodroplet regime. Our measurements are in good agreement with numerical calculations taking into account finite size effects.

DOI: 10.1103/PhysRevLett.132.103401

The successful production of degenerate quantum gases of magnetic lanthanide atoms [1,2] has opened the door to study the physics of strongly dipolar Bose-Einstein condensates (BECs), which is fundamentally altered by the long-range and anisotropic dipole-dipole interaction (DDI). The competition between the contact and dipolar interactions, together with a stabilization mechanism based on quantum fluctuations (QF) [3–9], gives rise to the appearance of a wide range of new exotic states, such as macrodroplets, droplet arrays, and supersolids; see Refs. [10,11] and references therein.

One of the keys to understanding both the stationary and the out-of-equilibrium properties of dipolar phases lies in the knowledge of their spectrum of collective excitations. Remarkably, the spectrum acquires a distinct momentum dependence due to the DDI, which is sensitive to the orientation of the dipoles with respect to the trap axis. As an example, we consider a dipolar BEC confined in a cigar-shaped harmonic trap with the weak axis along y. If the dipole orientation is perpendicular to y and the DDI is strong enough, then the spectrum of excitations develops a local minimum at finite momentum [12], called *roton* in analogy with helium superfluid [13]; see Fig. 1(a). This phenomenon, recently observed in experiments [14,15], is a direct consequence of the change of sign of the DDI from mainly repulsive to attractive for increasing momentum k_y. The ratio $\epsilon_{dd} = a_{dd}/a_s$, with a_{dd} and a_s being the dipolar and s-wave scattering lengths respectively, controls the roton energy gap. By increasing ϵ_{dd}, the energy of the roton mode can be decreased until the point where it completely softens, giving rise to the formation of supersolids and independent droplet states [11].

In the complementary case, where the dipole moment is aligned along y, the DDI is attractive for small k_y and rapidly becomes repulsive as k_y increases. Here, the condensate smoothly enters into a macrodroplet state [16] when increasing ϵ_{dd} above unity [8,9]. In this regime, the spectrum of excitations is much less explored. Just recently, theoretical works have revealed remarkable features: The excitation spectrum undergoes a stiffening, i.e. an upward curvature at low k_y, and a multiband response to excitations [17–19]; see Fig. 1(b). These distinct characteristics, denoted as the *antiroton* effect [18], call for an experimental verification as they play a crucial role in shaping the properties of macrodroplet states. Specifically, the observed stiffening at low k and the spreading of the

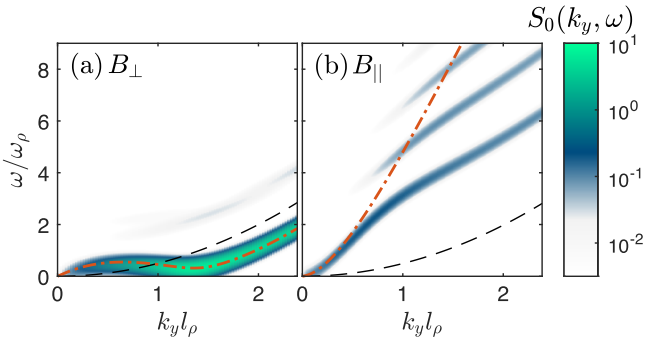

FIG. 1. Spectra of excitations of an infinitely elongated dipolar quantum gas in the roton (a) and antiroton regime (b), corresponding to dipoles oriented perpendicular or parallel to the long axis of the system, respectively. The calculations are performed for ^{166}Er in an infinite tube with transversal trapping frequency $\omega_\rho = 2\pi \times 198$ Hz, a uniform density of $n = 2.3 \times 10^3\ \mu\text{m}^{-1}$, where $\epsilon_{dd} = 1.36$ for (a) and $\epsilon_{dd} = 1.15$ for (b). The color map shows the strength of the zero-temperature dynamical structure factor S_0. The red dashed line is the variational energy [see Eq. (2)] and the black dashed line is the free particle energy ϵ_{k_y}. For visibility, a typical experimental Fourier broadening of 47 Hz is applied to the DSF.

system's response over multiple bands indicates the heightened resilience of a dipolar macrodroplet against excitations. This increased stability could potentially lead to the self-evaporation of these excitations, introducing a novel and intriguing aspect to the behavior of quantum systems bound by beyond-mean-field quantum fluctuations, as seen in dipolar gases and self-bound states in nondipolar mixtures [20–25].

In the present work we report on the experimental observation of the antiroton effect by measuring the excitation spectrum of an erbium quantum gas across the BEC-macrodroplet crossover. Furthermore, we extend the current theory to finite systems to determine the mechanisms underlying the peculiar shape of the spectrum. Not only do we observe the predicted stiffening of the lowest excitation branch at low k_y, we also measure a strong multiband response when increasing the imparted momentum.

To illustrate the physics of the antiroton, let us first discuss the theoretical framework to determine the excitation spectrum of a dipolar quantum gas in an infinite tube with constant density. The dynamic structure factor (DSF) $S(\mathbf{k},\omega)$ quantifies the density response of a system to a density-coupled scattering probe of momentum $\hbar\mathbf{k}$ and energy $\hbar\omega$ within linear response theory. For a BEC the DSF at $T = 0$ K is given by

$$S_0(\mathbf{k},\omega) = \sum_j \left| \int d\mathbf{x}(u_j^* + v_j^*) e^{i\mathbf{k}\cdot\mathbf{x}} \psi_0 \right|^2 \delta(\hbar\omega - \epsilon_j), \quad (1)$$

where $\{u_j(\mathbf{x}), v_j(\mathbf{x})\}$ are the Bogoliubov quasiparticle amplitudes with respective energies ϵ_j, and ψ_0 is the condensate wave function. As presented in Refs. [18,19], the excitations are plane waves along the y direction of the infinite tube i.e. $u_j(\mathbf{x}) \to \mathrm{u}_{\nu,k_y}(\boldsymbol{\rho}) e^{ik_y y}$, with ν labeling the transverse excitation (e.g. see Ref. [17]), $\hbar k_y$ being the y component of momentum, and $\boldsymbol{\rho} = (x, z)$ the transverse coordinates. Together with a variational description of the transverse structure of the condensate and excitations, this ansatz allows a simple semianalytical expression of the dispersion relation for the lowest excitation branch of the form

$$\epsilon_{k_y}^{\mathrm{var}} = \sqrt{\epsilon_{k_y}\left[\epsilon_{k_y} + 2n\tilde{U}_\alpha(k_y) + 3n^{3/2} g_{\mathrm{QF}}\right]}. \quad (2)$$

Here, $\epsilon_{k_y} = \hbar^2 k_y^2/2m$ and the quantities $\tilde{U}_\alpha(k_y)$ and g_{QF} describe the (Fourier transform of the) two-body interactions and the effects of quantum fluctuations after the transverse degrees of freedom are integrated out [26].

In the roton regime (dipoles perpendicular to y), the variational dispersion relation provides an excellent description of the full excitation spectrum, as shown by the remarkable agreement between Eq. (2) and the full numerical calculation, see Fig. 1(a). The latter, described in detail in the Supplemental Material [26] and Ref. [15], also reveals that the dynamic response of the system essentially involves only the lowest branch.

In the macrodroplet regime (dipoles parallel to y), the situation is very different. As shown in Fig. 1(b), Eq. (2) is only capable to describe the low momentum part ($k_y < 1/l_\rho$), where $l_\rho = \sqrt{\hbar/m\omega_\rho}$ is the characteristic transverse length scale and ω_ρ the transverse trapping frequency. For larger momenta, the variational dispersion relation deviates substantially from the numerics. Moreover, from the full calculation of the DSF, we also observe a strong multibranch response of the system for $k_y \gtrsim 1/l_\rho$ i.e. the DSF for a single momentum features multiple resonant energies with weights on the same order of magnitude. Both aspects suggest the emergence of new phenomena not captured by the above variational method. We find that the same qualitative behavior persists also in the experimentally relevant case of a three-dimensional trapped system. Despite the expected broadening and discretization of the excitation modes, the *antiroton* features are still visible, namely the stiffening of the spectrum with an initial rapid increase in energy with k_y and the strong multibranch response above $k_y \gtrsim 1/l_\rho$.

To probe the theoretical findings, we experimentally explore the spectrum of excitations of a macrodroplet state using Bragg spectroscopy. We first prepare a dipolar BEC of ^{166}Er in the lowest Zeeman state at a magnetic field of $\mathbf{B} = 1.9$ G pointing along z in a crossed dipole trap, analogous to Refs. [9,14]. We then prepare the state of interest by simultaneously rotating the direction of $\mathbf{B}$ to point toward y, ramping its magnitude to the desired value, and by reshaping the trap to $\omega_{x,y,z}/2\pi = (170, 30, 230)$ Hz, resulting in a characteristic transverse trapping frequency $\omega_\rho = \sqrt{\omega_x \omega_z} = 2\pi \times 198$ Hz with a corresponding length scale of $l_\rho = 0.55$ μm. Finally, we perform Bragg spectroscopy [33] by illuminating the cloud with a moving lattice with wave vector $\mathbf{k}_L = \mathbf{k}_1 - \mathbf{k}_2$ and angular frequency $\omega_L = \omega_1 - \omega_2$, resulting in a phase velocity of $v_L = \omega_L/|\mathbf{k}_L|$, see Fig. 2(a) [26].

In the experiment, $\mathbf{k}_L$ is aligned along y such that $\mathbf{k}_L = k_L \hat{\mathbf{y}}$. The lattice is created by letting two laser beams ($\mathbf{k}_1$, ω_1) and ($\mathbf{k}_2$, ω_2), red-detuned by about 40Γ from the main electronic transition of erbium at 401 nm, intersect at an angle θ at the position of the atoms. The two beams drive a two-photon transition when the resonance condition $\hbar\omega_L = \epsilon(k_L)$ is met, transferring momentum k_L and energy $\hbar\omega_L$ to the atoms. The imparted momentum and energy can be independently controlled via the digital micromirror device used to create both beams. We use a pulse duration of $\tau = 8.3$ ms, corresponding to roughly a quarter of the axial trap period, as a compromise between minimizing Fourier broadening and the influence of the trap on the momentum of the excited atoms. The power of the Bragg beams is chosen for each measurement in a range of

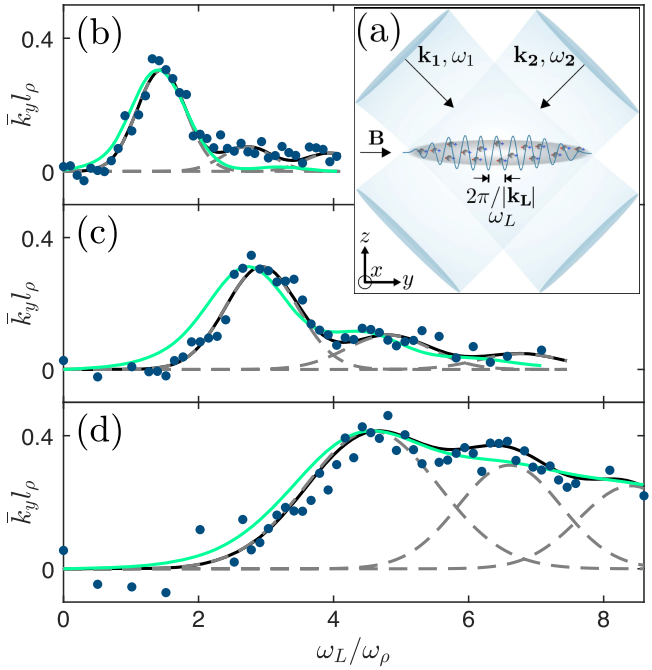

FIG. 2. (a) Illustration of the experimental setup: A BEC of ^{166}Er in an elongated trap with the dipole moment aligned along the weak axis y. Bragg spectroscopy is performed by intersecting two beams at the BEC which impart momentum $\hbar\mathbf{k}_L$ and energy $\hbar\omega_L$. (b)–(d) Measured response of the system $\bar{k}_y$ as a function of the excitation frequency ω_L/ω_ρ for three different values of the imparted momentum $k_L = [0.59, 1.0, 1.76]/l_\rho$, respectively. The black line is the sum of three Gaussians (dashed lines) fit to the data. The green lines are the theoretically calculated values of $S_0(k_y, \omega)$, rescaled in amplitude and accounting for the experimental Fourier and Doppler broadening.

1–7 mW such that a clear excitation signal is seen on resonance while the maximum excited fraction is kept below 20%. We probe the atomic cloud by standard absorption imaging along z after a total 30 ms time-of-flight (TOF) expansion. Excitations are then visible either as a separated peak for large k_L, or as an asymmetric broadening of the momentum distribution for low k_L. A more detailed description of our Bragg-spectroscopy setup based on a digital micromirror device can be found in Ref. [15].

From the 2D momentum distribution—assuming ballistic expansion during TOF—we extract the momentum profile along y by integrating out the x-direction $n(k_y) = \int n(k_x, k_y) dk_x$, and then calculate the mean momentum per particle as $\bar{k}_y = \int k_y n(k_y) dk_y / \int n(k_y) dk_y$ [26]. One can show that this quantity is directly proportional to the zero-temperature dynamical structure factor $S_0(\mathbf{k}, \omega)$ in the linear response regime as

$$\bar{k}_y = k_L \frac{\pi \tau V_0^2}{2\hbar} S_0(k_L, \omega), \tag{3}$$

where V_0 is the depth of the moving lattice [34,35]. This comparison between the mean imparted momentum and the dynamic structure factor is particularly robust since it is insensitive to scattering processes during or after the excitation pulse and does not rely on any fitting parameters [26].

Figures 2(b)–2(d) shows examples of the measured response of the system $\bar{k}_y$ as a function of the excitation frequency ω_L/ω_ρ for three different values of the imparted momentum k_L. At low momentum ($k_L = 0.59/l_\rho$), we observe one prominent resonance around $\omega_L \approx 1.5\omega_\rho$ indicating the presence of a single excitation branch. For larger momenta ($k_L = [1.0, 1.76]/l_\rho$), we instead observe a multipeak response, signalling that additional resonances at higher energies start to appear and become more pronounced when increasing k_L, see Figs. 2(c) and 2(d). A direct comparison of our experimental spectra to the expected response of the system from the full calculation reveals a good agreement with both energies and strengths of the excitation resonances when we take into account the expected Doppler and Fourier broadening [26]. While the Fourier broadening of $\delta\omega_F/2\pi \approx 47$ Hz does not depend on the probing momentum and determines the resonance width at low k_L, the Doppler broadening increases with k_L like $\delta\omega_D/2\pi \approx 58\ \text{Hz} \times k_L l_\rho$, limiting our ability to observe separated excitation branches due to their increasing spectral width.

We reconstruct the full spectrum of excitations by repeating the above measurements over a wide tuning range of $k_L = [0.06, 2.38]/l_\rho$. Figure 3 summarizes our experimental results together with the numerical calculations. The measured spectrum of excitations [Fig. 3(a)] shows the predicted steep upward curvature of the first excitation branch for low k_L, with an additional decrease of its slope and the appearance of a strong multiband response for increasing momentum. The datapoints mark our extracted resonance positions obtained by fitting multiple Gaussians to the obtained spectra for fixed k_L as shown in Figs. 2(b)–2(d).

Figure 3(b) shows our experimental results on top of the calculated DSF taking into account the expected Doppler and Fourier broadening as direct comparison, while Fig. 3(c) plots the bare theory spectrum without any broadening as reference. We find very good agreement between our experimental results and the numerical calculations, confirming the existence of the antiroton phenomena, which signalizes the macrodroplet's resilience to excitations. This rigidity is expected to further increase when moving from the BEC toward the macrodroplet regime [19]. This behavior becomes apparent from our study, showing that an ever-increasing energy is needed to excite the system as ϵ_{dd} increases. Figure 4(a) summarizes these findings. Here, for each point, we experimentally Bragg excite the system at a fixed momentum $k_L = 1.30/l_\rho$ and extract the excitation frequency belonging to the lowest

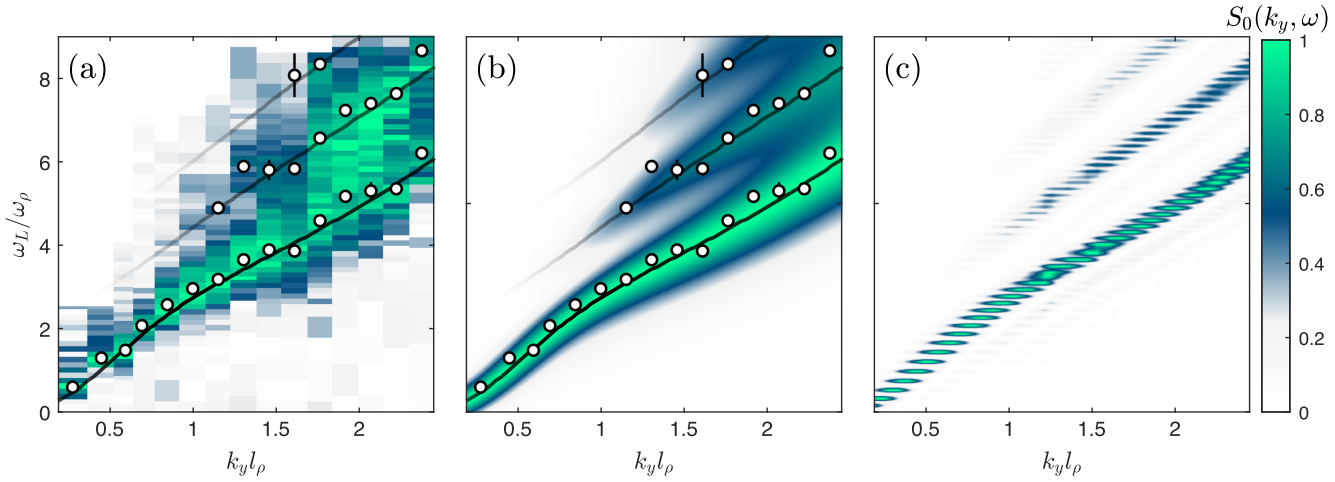

FIG. 3. Excitation spectrum of an elongated ^{166}Er cloud polarized along the weakly confined axis with $\epsilon_{dd} = 1.13$, $N = 25(5.0) \times 10^4$ and trapping frequencies $\omega_{x,y,z}/2\pi = (170, 30, 230)$ Hz. (a) Measured response of the system $\bar{k}_y$ as a function of ω_L/ω_ρ and k_L. The datapoints denote the experimentally detected resonance positions from fits as shown in Figs. 2(b)–2(d) with the error bars indicating one standard error from the fit. The black lines represent the maxima of $S_0(k_y, \omega)$ from our numerical calculation. (b) Detected resonance positions on top of the calculated $S_0(k_y, \omega)$ as indicated by the color map, including Fourier and Doppler broadening. (c) Calculated $S_0(k_y, \omega)$ for our finite system with minimal broadening. (a)–(c) Each momentum column is normalized to the maximum value.

branch of the spectrum. We then repeat the measurement for various interaction parameters in the range $\epsilon_{dd} = [0.73, 1.12]$ and observe the expected increase of excitation energy with increasing ϵ_{dd} in quantitative agreement to theory.

While the results clearly show the stiffening and dispersion of the response of a macrodroplet over multiple branches of excitation, the physical origin of this phenomenon and the reason for the failure of the variational approach still await explanation. We find that a first important indication comes from the theoretical study of the transverse behavior of the system. While the variational approach [Eq. (2)] imposes a Gaussian-type transverse profile of the excitation modes, regardless of energy, the numerical results show a marked change in the profile at low and high energy. This observation is exemplified in Figs. 4(b) and 4(c), in which we compare the profile of the density fluctuations $|\delta n|^2$ for specific excitation modes in the lowest branch at different energies ϵ_j. From the profile integrated along the axial direction, we observe that for increased energy the *transversal* profile of the excitation mode changes from a Gaussian-like shape to a more broadened multipeak structure, substantially differing from the ground-state wave function. This leads to a drastic reduction of the strength of the DSF of the lowest branch, since it scales directly with the overlap integral between the condensate and the excitation wave functions, see Eq. (1). As a consequence, the higher branches pick up more relative weight due to the f-sum rule [36], leading to the multiband response. This behavior of the shape also explains the breakdown of the variational model, as it assumes a similar transverse structure for the excitations and the condensate which is only valid for small energies in this regime.

But why do the excitations change their shape in the first place? Here one should be reminded that dipolar interactions exhibit a momentum dependence. In the macrodroplet regime, DDI are becoming attractive for small momenta and strongly repulsive for large momenta. Therefore excitations with large momentum exhibit a large

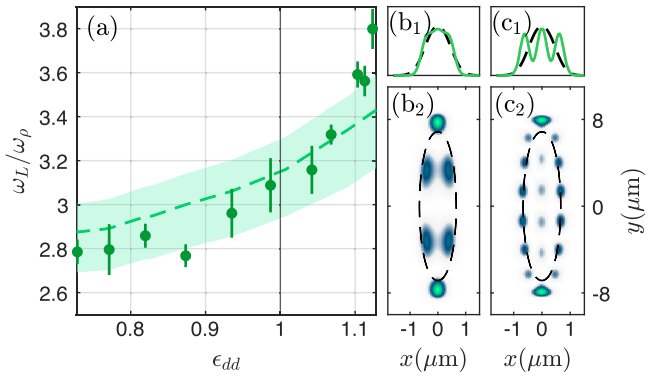

FIG. 4. Stiffening and shapes of excitation modes. (a) Frequency of the first excitation branch versus ϵ_{dd} at fixed excitation momentum $k_L = 1.30/l_\rho$. The error bars denote one standard error from the fit. The shaded area corresponds to the theoretical predictions within a range of atom number $N = [15, 35] \times 10^4$. (b_2),(c_2) Shapes of the numerically calculated excitation modes at $\epsilon_{dd} = 1.13$ and energies $\epsilon_j/\hbar = 0.51\omega_\rho$ (b) and $\epsilon_{j'}/\hbar = 1.87\omega_\rho$ (c) represented via plots of $|\delta n_j|^2 = |(u_j^* + v_j^*)\psi_0|^2$. The dashed lines mark the 1/e size of the condensate. (b_1),(c_1) Profiles of the excitation modes after integration along y. The dashed lines mark the integrated shape of the condensate.

repulsion from the condensate, forcing them to reduce their overlap to lower the energy. This goes hand-in-hand with the transition from collective to single-particle excitations as the excitation energy increases above the chemical potential μ of the condensate [36].

In summary, this work presents the first measurement of the excitation spectrum of a dipolar quantum gas in the crossover regime from a Bose-Einstein condensate to a macrodroplet state. While a dominant side-by-side dipole orientation typically leads to a softening of the excitation spectrum, resulting in the emergence of the roton spectrum [12,14] and eventually supersolidity [11], our observations reveal a contrary behavior. Specifically, we note a stiffening of the excitation spectrum and a spreading of the dynamic structure factor across multiple branches when dipoles are primarily arranged head to tail. This phenomenon, referred to as the antiroton effect, becomes particularly pronounced in the macrodroplet phase, imparting a resistance to the formation of density modulations.

Our findings open the path for further investigation into the excitations of the macrodroplet and their impact on the system's behavior, especially in the self-bound regime. In this scenario, it is predicted [17,19] that reducing the confinement will transform the multiple discrete branches that couple to axial probing into just one discrete branch and a continuum of excitations. The observed increased stiffening is also predicted to induce self-evaporation of excitations [37], prompting questions about interpreting finite temperature effects in such systems. Another unresolved aspect is whether the system has a critical velocity and its relation to the incompressible nature of the droplet [19].

We acknowledge T. Mézières, L. Lafforgue, and L. Chomaz for discussion and support in the early stages of the experiment. We are grateful to T. Bland and E. Poli for helpful discussions about the theoretical simulations. The Innsbruck team acknowledges support from the European Research Council through the Advanced Grant DyMETEr (No. 101054500), the DFG/FWF via FOR 2247/I4317-N36, and a NextGeneration EU grant AQuSIM by the Austrian Research Promotion Agency FFG (No. FO999896041). A. H. acknowledges funding from the Austrian Science Fund (FWF) within DK-ALM (No. W1259-N27). D. B. and P. B. B. acknowledge support from the Marsden Fund of the Royal Society of New Zealand (MFP-22-UOO-011).

[1] M. Lu, N. Q. Burdick, S. H. Youn, and B. L. Lev, Strongly dipolar Bose-Einstein condensate of dysprosium, Phys. Rev. Lett. **107**, 190401 (2011).

[2] K. Aikawa, A. Frisch, M. Mark, S. Baier, A. Rietzler, R. Grimm, and F. Ferlaino, Bose-Einstein condensation of erbium, Phys. Rev. Lett. **108**, 210401 (2012).

[3] H. Kadau, M. Schmitt, M. Wenzel, C. Wink, T. Maier, I. Ferrier-Barbut, and T. Pfau, Observing the Rosensweig instability of a quantum ferrofluid, Nature (London) **530**, 194 (2016).

[4] I. Ferrier-Barbut, H. Kadau, M. Schmitt, M. Wenzel, and T. Pfau, Observation of quantum droplets in a strongly dipolar Bose gas, Phys. Rev. Lett. **116**, 215301 (2016).

[5] F. Wächtler and L. Santos, Quantum filaments in dipolar Bose-Einstein condensates, Phys. Rev. A **93**, 061603(R) (2016).

[6] R. N. Bisset, R. M. Wilson, D. Baillie, and P. B. Blakie, Ground-state phase diagram of a dipolar condensate with quantum fluctuations, Phys. Rev. A **94**, 033619 (2016).

[7] D. Baillie, R. M. Wilson, R. N. Bisset, and P. B. Blakie, Self-bound dipolar droplet: A localized matter wave in free space, Phys. Rev. A **94**, 021602(R) (2016).

[8] M. Schmitt, M. Wenzel, F. Böttcher, I. Ferrier-Barbut, and T. Pfau, Self-bound droplets of a dilute magnetic quantum liquid, Nature (London) **539**, 259 (2016).

[9] L. Chomaz, S. Baier, D. Petter, M. J. Mark, F. Wächtler, L. Santos, and F. Ferlaino, Quantum-fluctuation-driven crossover from a dilute Bose-Einstein condensate to a macrodroplet in a dipolar quantum fluid, Phys. Rev. X **6**, 041039 (2016).

[10] M. A. Norcia and F. Ferlaino, Developments in atomic control using ultracold magnetic lanthanides, Nat. Phys. **17**, 1349 (2021).

[11] L. Chomaz, I. Ferrier-Barbut, F. Ferlaino, B. Laburthe-Tolra, B. L. Lev, and T. Pfau, Dipolar physics: A review of experiments with magnetic quantum gases, Rep. Prog. Phys. **86**, 026401 (2022).

[12] L. Santos, G. V. Shlyapnikov, and M. Lewenstein, Roton-Maxon spectrum and stability of trapped dipolar Bose-Einstein condensates, Phys. Rev. Lett. **90**, 250403 (2003).

[13] L. D. Landau, The theory of superfluidity of helium II, J. Phys. (Moscow) **5**, 71 (1941).

[14] L. Chomaz, R. M. W. van Bijnen, D. Petter, G. Faraoni, S. Baier, J. H. Becher, M. J. Mark, F. Wächtler, L. Santos, and F. Ferlaino, Observation of roton mode population in a dipolar quantum gas, Nat. Phys. **14**, 442 (2018).

[15] D. Petter, G. Natale, R. M. W. van Bijnen, A. Patscheider, M. J. Mark, L. Chomaz, and F. Ferlaino, Probing the roton excitation spectrum of a stable dipolar Bose gas, Phys. Rev. Lett. **122**, 183401 (2019).

[16] A macrodroplet state is defined as the ground state of a dipolar gas that exists due to the stabilization of quantum fluctuations, where by contrast mean-field theory (standard GPE) would predict a collapse of the dipolar gas. A macrodroplet can in addition become self-bound by further decreasing the contact interaction.

[17] D. Baillie, R. M. Wilson, and P. B. Blakie, Collective excitations of self-bound droplets of a dipolar quantum fluid, Phys. Rev. Lett. **119**, 255302 (2017).

[18] S. Pal, D. Baillie, and P. B. Blakie, Excitations and number fluctuations in an elongated dipolar Bose-Einstein condensate, Phys. Rev. A **102**, 043306 (2020).

[19] S. Pal, D. Baillie, and P. B. Blakie, Infinite dipolar droplet: A simple theory for the macrodroplet regime, Phys. Rev. A **105**, 023308 (2022).

[20] C. R. Cabrera, L. Tanzi, J. Sanz, B. Naylor, P. Thomas, P. Cheiney, and L. Tarruell, Quantum liquid droplets in a

mixture of Bose-Einstein condensates, Science **359**, 301 (2018).

[21] P. Cheiney, C. R. Cabrera, J. Sanz, B. Naylor, L. Tanzi, and L. Tarruell, Bright soliton to quantum droplet transition in a mixture of Bose-Einstein condensates, Phys. Rev. Lett. **120**, 135301 (2018).

[22] G. Semeghini, G. Ferioli, L. Masi, C. Mazzinghi, L. Wolswijk, F. Minardi, M. Modugno, G. Modugno, M. Inguscio, and M. Fattori, Self-bound quantum droplets of atomic mixtures in free space, Phys. Rev. Lett. **120**, 235301 (2018).

[23] G. Ferioli, G. Semeghini, L. Masi, G. Giusti, G. Modugno, M. Inguscio, A. Gallemí, A. Recati, and M. Fattori, Collisions of self-bound quantum droplets, Phys. Rev. Lett. **122**, 090401 (2019).

[24] A. Burchianti, C. D'Errico, M. Prevedelli, L. Salasnich, F. Ancilotto, M. Modugno, F. Minardi, and C. Fort, A dual-species Bose-Einstein condensate with attractive interspecies interactions, Condens. Matter **5**, 21 (2020).

[25] F. Böttcher, J.-N. Schmidt, J. Hertkorn, K. S. H. Ng, S. D. Graham, M. Guo, T. Langen, and T. Pfau, New states of matter with fine-tuned interactions: Quantum droplets and dipolar supersolids, Rep. Prog. Phys. **84**, 012403 (2020).

[26] See Supplemental Material at http://link.aps.org/supplemental/10.1103/PhysRevLett.132.103401 for details on the variational model, the experimental procedure and data analysis as well as a comparison between the DSF $S(q,\omega)$ and our observable $\bar{k}_y$. The Supplemental Material includes Refs. [27–32].

[27] P. B. Blakie, D. Baillie, and S. Pal, Variational theory for the ground state and collective excitations of an elongated dipolar condensate, Commun. Theor. Phys. **72**, 085501 (2020).

[28] A. R. P. Lima and A. Pelster, Quantum fluctuations in dipolar Bose gases, Phys. Rev. A **84**, 041604(R) (2011).

[29] G. Veeravalli, E. Kuhnle, P. Dyke, and C. J. Vale, Bragg spectroscopy of a strongly interacting Fermi gas, Phys. Rev. Lett. **101**, 250403 (2008).

[30] F. Zambelli, L. Pitaevskii, D. M. Stamper-Kurn, and S. Stringari, Dynamic structure factor and momentum distribution of a trapped Bose gas, Phys. Rev. A **61**, 063608 (2000).

[31] D. M. Stamper-Kurn, A. P. Chikkatur, A. Görlitz, S. Inouye, S. Gupta, D. E. Pritchard, and W. Ketterle, Excitation of phonons in a Bose-Einstein condensate by light scattering, Phys. Rev. Lett. **83**, 2876 (1999).

[32] J. Steinhauer, R. Ozeri, N. Katz, and N. Davidson, Excitation spectrum of a Bose-Einstein condensate, Phys. Rev. Lett. **88**, 120407 (2002).

[33] J. Stenger, S. Inouye, A. P. Chikkatur, D. M. Stamper-Kurn, D. E. Pritchard, and W. Ketterle, Bragg spectroscopy of a Bose-Einstein condensate, Phys. Rev. Lett. **82**, 4569 (1999).

[34] A. Brunello, F. Dalfovo, L. Pitaevskii, S. Stringari, and F. Zambelli, Momentum transferred to a trapped Bose-Einstein condensate by stimulated light scattering, Phys. Rev. A **64**, 063614 (2001).

[35] P. B. Blakie, R. J. Ballagh, and C. W. Gardiner, Theory of coherent Bragg spectroscopy of a trapped Bose-Einstein condensate, Phys. Rev. A **65**, 033602 (2002).

[36] L. Pitaevskii and S. Stringari, *Bose-Einstein Condensation and Superfluidity* (Oxford University Press, New York, 2016), Vol. 164.

[37] D. S. Petrov, Quantum mechanical stabilization of a collapsing Bose-Bose mixture, Phys. Rev. Lett. **115**, 155302 (2015).